Using thermo-optical nonlinearity to robustly separate absorption and radiation losses in nanophotonic resonators: supplement

MINGKANG WANG,[1,2,3] **DIEGO J. PEREZ-MORELO,**[1,2] **AND VLADIMIR A. AKSYUK**[1,4]

[1]*Microsystems and Nanotechnology Division, National Institute of Standards and Technology, Gaithersburg, MD 20899, USA*
[2]*Institute for Research in Electronics and Applied Physics, University of Maryland, College Park, MD 20742, USA*
[3]*mingkang.wang@nist.gov*
[4]*vladimir.aksyuk@nist.gov*

Supplementary Materials

Using thermo-optical nonlinearity to robustly separate absorption and radiation losses in nanophotonic resonators

Mingkang Wang[1,2, †], Diego J. Perez-Morelo[1,2], Vladimir Aksyuk[1, *]

[1]Microsystems and Nanotechnology Division, National Institute of Standards and Technology, Gaithersburg, MD 20899 USA

[2]Institute for Research in Electronics and Applied Physics, University of Maryland, College Park, MD 20742, USA

1. Numerical simulation of the thermal effect

As described in the main text, our nominally 10 µm diameter, 260 nm thick silicon microdisk is supported at the center by a 2 µm thick silica post. The diameter of the top and bottom surface of the post defined by the hydrofluoric acid etching process is measured to be ≈ 1.5 µm and ≈ 2.2 µm. The whole setup is in an air environment.

In the simulation, an input power of $P_{in} \approx 0.1$ mW is applied at time zero to the rim of the microdisk where the optical modes are located. Figure S1 (a) shows the temperature distribution of the system at the thermal equilibrium. The post is the main source of thermal impedance, while the Si substrate has high-enough thermal conductivity to be nearly isothermal. The effect of the cantilever on the simulation results is less than 2%, however, for the accuracy, we also included the cantilever in the model. The time-domain thermal simulation result is presented in Figure S1

(b). By fitting the curve with $T = T' + \Delta T e^{-\frac{t}{\tau}}$, we obtain the thermal response time $\tau \approx 7.0$ µs, and

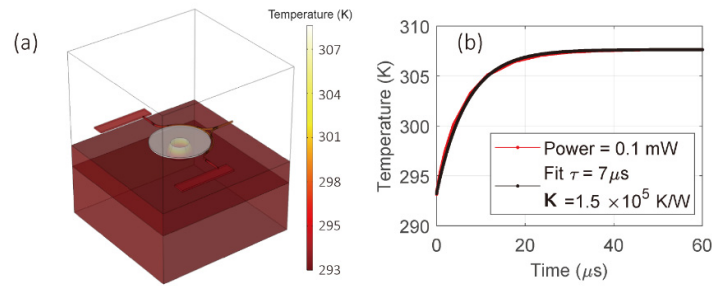$\kappa = \frac{\Delta T}{P_{in}} \approx 1.5 \times 10^5$ K/W. $T' = 293$ K is a constant offset.

Figure S1. Simulated thermal response of the silicon microdisk. (a). Thermal distribution on the microdisk at equilibrium. (b). Dynamic response of the disk to the application of a known thermal load at the periphery.

2. Extraction of thermal time constant via intensity modulation

As thermal time constants in nanophotonic resonators may be several microseconds or longer, frequency modulation via phase electro-optical modulators (EOM) requires deep phase modulation that is challenging to implement. Therefore we implement a method that extracts the thermal time constant based on much more easily achievable intensity modulation,. The method

relies on the interplay between the optical response and the thermodynamics in nanophotonic resonators via thermo-optical effect. As shown in Figure S2 (a), if the input optical intensity is reduced by ΔI_0, the transmission intensity at the resonance (red dot) will first reduce to the scaled solid blue line quickly, and then slowly decay to the dashed blue line due to the thermo-optical tuning of resonance. Note, Fig. S2 (a) exaggerates the intensity modulation for a better presentation, the actual modulation is just a perturbation ($\Delta I_0 \ll I_0$). The tuning-induced variation of the transmission can be simply understood, as that the decrease of intensity lowers the temperature in the resonator, shifting the resonance wavelength by $\Delta\lambda$ to a lower wavelength. The resonance shift leads to extra intensity change proportional to $\Delta\lambda$. Furthermore, $\Delta\lambda$ is proportional to ΔT based on Eq. (2). Considering the two parts, we have:

$$\Delta I = k\Delta I_0 + p\Delta T \tag{S1}$$

where ΔI is the intensity variation at the resonance due to intensity modulation ΔI_0, k and p are two proportionality constants, ΔT is the temperature variation in the nanophotonic resonator and it can be expressed by the thermodynamic equation:

$$\frac{d(\Delta T)}{dt} = -\frac{1}{\tau}(\Delta T - \Delta I_0) \tag{S2}$$

where τ is the thermal time constant and we express the temperature change ΔT in the units of intensity change ΔI_0 for simplicity of notation ($\Delta T = \Delta I_0$ defines the steady state relationship of temperature on intensity change). Finally, we write the intensity modulation as harmonic drive, and the resulting intensity and temperature changes are also in the harmonic form:

$$\begin{aligned} \Delta I_0 &= \widehat{I_0}e^{i\omega t} \\ \Delta I &= \hat{I}e^{i\omega t} \\ \Delta T &= \hat{T}e^{i\omega t} \end{aligned} \tag{S3}$$

By applying Eq. (S3) to (S1) and (S2), we obtain the amplitude $\hat{I}$ as:

$$\hat{I} = \widehat{I_0}\left(k + \frac{p}{1+i\omega\tau}\right) \tag{S4}$$

At $\omega \gg 1/\tau$, the thermodynamics cannot follow the quick modulation, so the thermal tuning effect (second term in Eq. S1) is negligible, $\hat{I} = k\widehat{I_0} = c_1$. At $\omega \ll 1/\tau$, the resonator is always at equilibrium, therefore, the amplitude of intensity is affected by the thermal effect: $\hat{I} = k\widehat{I_0} + p\widehat{I_0} = c_1 + c_2$. Since c_1 and c_2 can be measured individually, Eq. (S4) is simplifier to:

$$\hat{I} = c_1 + \frac{c_2}{1+i\omega\tau} \tag{S5}$$

In practice, rather than using a dedicated amplitude-modulating EOM, we have used a phase EOM to achieve amplitude modulation. This was possible due to the combination of the EOM's polarization-dependent phase modulation strength and the polarization-dependent fiber to photonic waveguide coupling. When the EOM input polarization is deliberately misaligned from the EOM principal axes and the EOM polarization principal axes are in turn misaligned from the on-chip waveguide input coupler axes, the TE and TM modes in the waveguide both acquire amplitude modulation. Only *TM* mode is coupled to the optical cavity modes under consideration, therefore the *TE* component is just a constant modulated intensity background independent from ω. Moreover, due to energy conservation, the intensity of *TE* is out of phase from the *TM* signal, providing a negative background $-b_1$ to the in-phase components of the phase sensitive readout. Therefore, the overall readout is:

$$\hat{I} = B_1 + \frac{c_2}{1+i\omega\tau} \tag{S6}$$
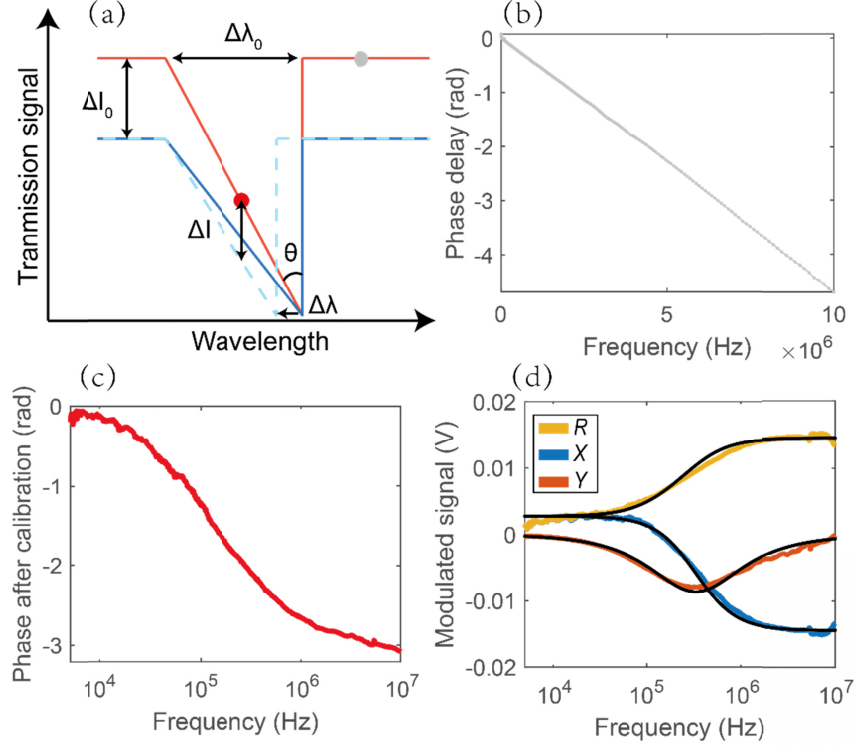
where $B_1 = c_1 - b_1$.

Figure S2. Characterization of the thermal time constant via intensity modulation. (a). Schematic of transmission signal under the intensity modulation. The change of transmission intensity at the working wavelength (red dot) contains two parts which are from the red line to the solid blue line and further to the dashed blue line. (b) Phase as a function of modulation frequency measured at the background (gray dot). (c) Calibrated phase as a function of modulation frequency measured at the working wavelength. (d) Measured modulated transmission intensity. Yellow, blue, and orange lines are amplitude R, in-phase component X, and out-of-phase component Y. The black lines are the fit of Eq. (S5)'s amplitude, real and imaginary parts.

In the experiment, we first measure the phase delay induced by the electric transmission line at the wavelength of the background (gray dot), shown as Fig.S2 (b), and use it to calibrate the phase of the signal measured at the working wavelength (red dot), shown as Fig.S2 (c). The amplitude, in-phase and out-of-phase parts of the calibrated signal are presented in Fig.S2 (d) as the yellow, blue, and orange dots, respectively. At the frequency of around 10 MHz, we get $B_1 \approx -14.5$ mV from the in-phase component, while at around 10 kHz we get $B_1 + c_2 \approx 2.8$ mV. With the known B_1 and c_2, we fit the in-phase component by Eq. (S6), and obtain $\tau = 6.8 \pm 0.3$ μS. To better present the *TM* part of the signal, we exclude the *TE* components by assuming *TM* and *TE* are nearly equal at low frequencies, so $b_1 \approx -20$ mV. This assumption does not affect the fitting procedure at all. In Figure 4, we add 20 mV to the in-phase component to exclude the *TE* part for a better presentation of the *TM* signal.

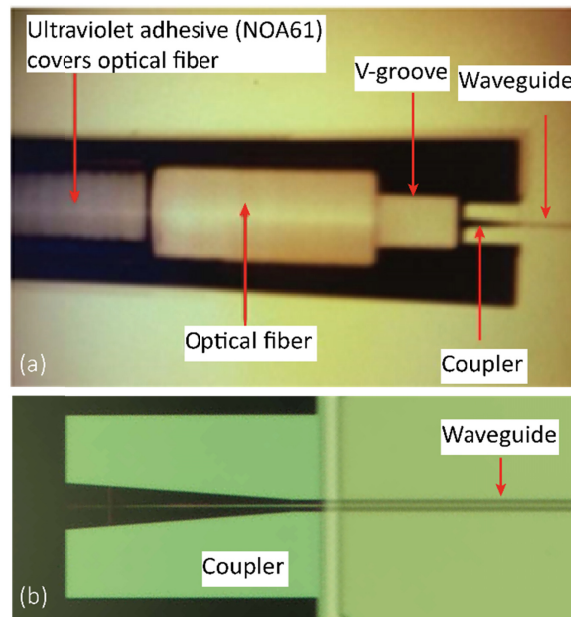3. **Coupling laser from optical fiber to on-chip waveguide**

Figure S3. Optical photo of input/output module of the device. The device contains two V-grooves etched by Cesium hydroxide on the Si device layer. One of the V-grooves is shown in (a) as an example. An optical fiber is glued in the V-groove by ultraviolet adhesive (NOA61). Laser from the optical fiber couples to the on-chip waveguide via a coupler. A zoomed-in photo is shown in (b). The detailed fabrication process can be found in our previous work Ref. [25].